

IMPULSIVE GENERATION OF VERTICAL OSCILLATIONS OF A SOLAR CORONAL ARCADE LOOP

M. Selwa¹, K. Murawski¹, S. K. Solanki², T. J. Wang², and U. Shumlak³

¹Institute of Physics, UMCS, ul. Radziszewskiego 10, 20-031 Lublin, Poland

²Max-Planck-Institut für Sonnensystemforschung, Max-Planck-Str. 2, 37191 Katlenburg-Lindau, Germany

³Aeronautics and Astronautics Department, University of Washington, Box 352250, Seattle, WA 98195-2250, USA

ABSTRACT

We consider impulsively generated oscillations of a solar coronal arcade loop. The two-dimensional ideal MHD numerical model we implement includes the effects of field line curvature and nonlinearity on the excitation and attenuation of standing fast magnetosonic waves. The results of the numerical simulations reveal wave signatures which are reminiscent of recent TRACE observational data. From our parametric studies we deduce that wave periods and attenuation times of the excited waves depend upon the position of the pulse below the loop summit, as well as its width and strength; wider pulses launched closer to a foot-point and to the loop apex trigger wave packets dominated by longer periods which are more strongly attenuated. We consider two kinds of attenuation mechanisms: wave leakage and geometric loop restructuring due to the initial pulse.

Key words: solar corona, MHD, oscillations.

1. INTRODUCTION

Magnetic loops are the main ingredients of the solar corona that sustain oscillations (e.g., Aschwanden et al. 1999, Wang et al. 2002, Wang & Solanki 2004). In one of the most recent observations Wang and Solanki (2004) reported on vertical oscillations of a 300 – 400 Mm long solar coronal loop which expanded and shrank with an oscillation period of ≈ 230 s, thus adding another mode of oscillation to those discovered earlier. Here we concentrate on modeling this mode of oscillation.

Recently, emphasis has been placed on the excitation of transverse waves. Transverse oscillations in solar coronal loops induced by propagating Alfvénic pulses were discussed by del Zanna et al. (2005). Fast standing waves were numerically simulated by Murawski et al. (2005a) who found high-order standing fast kink mode oscillations in a weakly magnetized coronal loop. In another context Murawski et al. (2005b) showed that impulsively

triggered fast magnetosonic waves in a cool loop (1 – 2 MK) have periods which are compatible with the observational data provided by TRACE which may be interpreted as the fast kink mode in the arcade. Selwa et al. (2005b) extended this model for a strongly magnetized coronal loop but they discussed only the case of a pulse launched centrally below the loop at the photospheric level while parametric studies are required to understand the complex scenario of loop oscillations.

A main goal of this paper is to perform parametric studies and extend the models of Murawski et al. (2005a,b) and Selwa et al. (2005b).

The paper is organized as follows: the numerical model is described in Sect. 2. The numerical results are presented in Sect. 3. This paper is concluded by a short summary of the main results in Sect. 4.

2. NUMERICAL MODEL

We describe coronal plasma by the ideal magnetohydrodynamic (MHD) equations:

$$\frac{\partial \varrho}{\partial t} + \nabla \cdot (\varrho \mathbf{V}) = 0, \quad (1)$$

$$\frac{\partial (\varrho \mathbf{V})}{\partial t} + \nabla \cdot [(\varrho \mathbf{V}) \mathbf{V}] = -\nabla p + \frac{1}{\mu} (\nabla \times \mathbf{B}) \times \mathbf{B}, \quad (2)$$

$$\frac{\partial E}{\partial t} + \nabla \cdot \left[(E + p_T) \mathbf{V} - \frac{\mathbf{B}(\mathbf{B} \cdot \mathbf{V})}{\mu} \right] = 0, \quad (3)$$

$$\frac{\partial \mathbf{B}}{\partial t} = \nabla \times (\mathbf{V} \times \mathbf{B}), \quad (4)$$

$$\nabla \cdot \mathbf{B} = 0. \quad (5)$$

Here μ is the magnetic permeability, ϱ is mass density, \mathbf{V} is flow velocity, p is gas pressure, \mathbf{B} is magnetic field, the symbol p_T denotes the total pressure that represents the sum of the gas and magnetic pressures:

$$p_T = p + \frac{B^2}{2\mu} \quad (6)$$

and plasma energy density is expressed as

$$E = \frac{\rho V^2}{2} + \frac{p}{\gamma - 1} + \frac{B^2}{2\mu}, \quad (7)$$

where γ is the adiabatic index.

2.1. Equilibrium configuration

We adopt and modify the coronal arcade model that was described recently by Selwa et al. (2005b). In this model the coronal arcade is settled in a two-dimensional, gravity-free and motionless environment. The equilibrium magnetic field $\mathbf{B}_e = [B_{ex}, 0, B_{ez}]$ has two non-zero components which are specified with the help of the vector magnetic potential $\mathbf{A} = A\hat{y}$ as

$$\mathbf{B}_e = \nabla A \times \hat{y}, \quad (8)$$

where \hat{y} is a unit vector along the y -direction and A satisfies Laplace's equation, $\nabla^2 A = 0$, whose solution is

$$A(x, z) = B_0 \Lambda_B \cos(x/\Lambda_B) e^{-z/\Lambda_B}. \quad (9)$$

From Eq. (8) we obtain then

$$B_{ex} = B_0 \cos(x/\Lambda_B) e^{-z/\Lambda_B}, \quad (10)$$

$$B_{ez} = -B_0 \sin(x/\Lambda_B) e^{-z/\Lambda_B}, \quad (11)$$

where B_0 is the magnetic field at the level $z = 0$ and Λ_B is the magnetic scale height such that

$$\Lambda_B = \frac{2L}{\pi}. \quad (12)$$

Here L is the horizontal half-width of the arcade, chosen as $L = 100$ Mm.

We consider one choice of background Alfvén speed $V_A = |B_e|/\sqrt{\mu\rho_e}$, where ρ_e is a background mass density. In this case V_A decays exponentially with height z and the background temperature $T_e \sim p_e/\rho_e$ is constant. Here $p_e = \text{const}$ is the background pressure.

Next we embed a loop in the arcade in such a way that its edges follow two specific magnetic field lines. We prescribe that the inner and outer field lines cross the base of the arcade at $|x| = L_f - 2a_f$ and $|x| = L_f$, respectively. Inside the loop we use the following density profile:

$$\rho(x, z) = d\rho_e(z) \left[H \left(\frac{A - A_2}{B_0 \Lambda_B} \right) - H \left(\frac{A - A_1}{B_0 \Lambda_B} \right) \right], \quad (13)$$

where $A_1 = A(L_f, 0) < A_2 = A(L_f - 2a_f, 0)$ and H is Heaviside's function. The mass density in this loop varies abruptly at its sides, leading to a density enhancement of the loop compared to the ambient medium. We choose the mass density contrast $d = \rho_i/\rho_e = 10$ with ρ_i and ρ_e corresponding to mass density respectively within the loop and in the ambient medium. As a reference we set $L_f = 0.7L$ and $a_f = 0.0125L$: they uniquely specify the

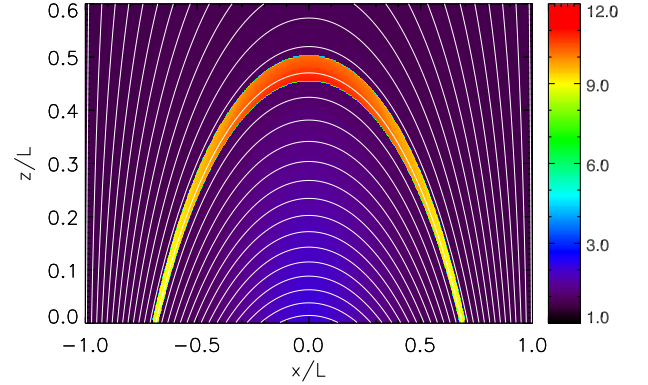


Figure 1. Initial configuration in the case of the pulse at $x_0 = z_0 = 0$. Mass density contours (colour scale, arbitrary units $\rho_e = 10^{-12}$ kg/m³) represent a loop denser than corona. Magnetic field lines are shown as solid white lines. Note that loop apex is denser than foot-points due to hot dense pulse.

loop's length l , height h and its width $2a$ at the summit. This loop does not have a perfect circular shape, but its average radius and length can be estimated as 70 Mm and 190 Mm, respectively (Fig. 1).

Due to the enhanced density, the Alfvén speed within the loop is smaller than its value in the ambient medium. As a result of this depression in the Alfvén speed the loop becomes a cavity for fast magnetosonic waves. We denote the Alfvén speed within the loop by $v_{Ai} = v_{Ae}/\sqrt{d}$.

Magnetic field at the photospheric level, B_0 , is connected to the reference mass density $\rho_e(0)$ through the reference Alfvén speed $V_{A0} = B_0/\sqrt{\mu\rho_e(0)}$, where we assume $\rho_e(0) = 10^{-15}$ kg m⁻³ and $V_{A0} = 1$ Mm s⁻¹ for the mass density and the Alfvén speed, respectively at the level $z = 0$.

For a potential magnetic arcade the equilibrium pressure p_e has to be constant. This pressure can be evaluated from the definition of the plasma $\beta = 2\mu p_e/B_e^2$. In this model in the ambient plasma, β grows from 0.012 at the loop foot-points to 0.054 at the loop apex. This growth is not quite realistic but the value of β remains below unity.

2.2. Perturbations

Perturbations in Eqs. (1)-(3) can be excited in such a loop in numerous ways. As we are interested in impulsively excited waves, we launch a hot pulse in the pressure and mass density, i.e.

$$\begin{aligned} \delta\rho(x, z, t = 0) &= A_\rho \rho_0 e^{-((x-x_0)^2 + (z-z_0)^2)/w^2}, \\ \delta p(x, z, t = 0) &= A_p p_0 e^{-((x-x_0)^2 + (z-z_0)^2)/w^2}, \end{aligned} \quad (14)$$

where w is the initial pulse width and (x_0, z_0) denotes its initial position. We choose initial relative amplitudes of the pulse $A_g = A_p/10$ which corresponds to a pulse that is 6.4 times hotter than the corona. It is noteworthy that the vertical oscillations seen by TRACE (Wang & Solanki 2004) are identified in gas at around 1 MK. We have no information of the temperature of the pulse causing this oscillation, although the gas in the oscillating loop does not appear to get heated by the pulse. In the absence of further information we adopt the above values of the amplitudes, which had been successfully employed by Selwa et al. (2005b), as reference values.

3. NUMERICAL RESULTS

The numerical code EMILY we adopt was developed by Jones et al. (1997). This code employs an explicit-implicit algorithm for solving the time-dependent, non-ideal magnetohydrodynamic equations. The algorithm is a finite-volume scheme that uses an approximate Riemann solver for the hyperbolic fluxes and central differencing applied on nested control volumes for the parabolic fluxes that arise from the non-ideal terms (i.e., resistivity and viscosity). This scheme is second-order accurate in space and time. In our studies we used the explicit option of the code for ideal magnetohydrodynamic equations.

Equations (1)-(5) are solved numerically in an Eulerian box with the x - and z -dimensions $(-L, L) \times (0, 2L)$. This box is covered by a uniform grid of 300×400 or 600×800 numerical cells. Grid convergence studies, which are based on grid refinement, are performed to show that the numerical results are not affected by insufficient spatial resolution. We apply open boundary conditions, with zero-gradient extrapolation of all plasma variables, at the right, left and top sides of the simulation region, thus allowing a wave signal to leave freely the simulation region. We set line-tying boundary conditions at the bottom of the simulation region. These boundaries model the interaction between the denser photosphere and the overlying plasma layers.

3.1. Pulses of various amplitudes

We begin our parametric studies with the pulse launched at $x_0 = z_0 = 0$. The pulse width $w = 35$ Mm and its amplitude $A_p = 15 p_e$ are fixed. Fig. 2 displays time-signatures of the mass density. These signatures are made by collecting the signal in time at the loop apex on the line $x = 0$. The moment $t = 0$ corresponds to the time at which the pulse is released at $z = 0$. The loop apex is initially displaced upward by $\sim 0.06 L$, which for the chosen value of $L = 10^2$ Mm corresponds to ~ 6 Mm, which is close to the observed displacement of 7.9 Mm (Wang & Solanki 2004). Except for the amplitude of the displacement the strength of the pulse does not have a significant effect on the properties of the oscillations. Note

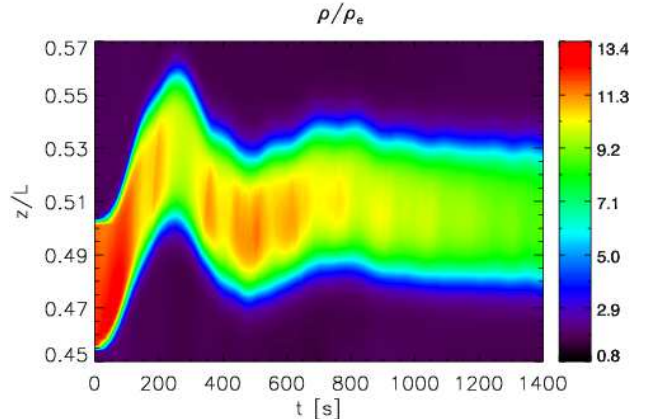


Figure 2. Time-signatures of the mass density at the loop apex for $A_p = 15 p_e$, $x_0 = z_0 = 0$. Spatial coordinates and time are measured in units of L and in seconds, respectively.

that the loop displays a reduction in density at the apex. It is noteworthy that the apex position along the z axis and density at the apex are anticorrelated (with correlation ratio -0.71). Note also the smaller amplitude, more rapid oscillations, which are also partly visible in the density. These were identified as sausage mode oscillations by Selwa et al. (2005b).

It is noteworthy that the loop does not return to its initial position, displaying an offset. This offset is a consequence of the loop in the simulations reaching a final equilibrium that is different from the initial one due to the non-potential shape component added by the pulse - while the initial magnetic field shape does not significantly change (there is no initial perturbation in the magnetic field), the density profile is slightly modified (the apex goes up and foot-points draw together as the density follows the Gaussian shape of the pulse), so the density does not exactly follow field lines. A similar behaviour is also seen in some TRACE data (Wang & Solanki 2004).

The oscillations seen in Fig. 2 represent the response of the loop summit to the initial perturbation. They correspond to a packet of waves among which kink waves exhibit the main contribution (Murawski et al. 2005a,b, Selwa et al. 2005b). As the signal in Fig. 2 decays with attenuation time τ , the wave period also evolves with time. From our simulation we get the values of the ratio $\tau/P \sim 0.5$. These periods and attenuation times are obtained by fitting the simulation time-signatures with attenuated sine functions (Selwa et al. 2005b).

3.2. Pulses along horizontal line $z_0 = 0$

In this part of the paper we discuss the case of pulses launched along a horizontal line that joins the two foot-points of the loop. Fig. 3 shows the time-signature of the

loop apex in response to a pulse launched in the neighborhood of the left foot-point. Fig. 3 shows some similarities but also considerable differences compared to Fig. 2. A kink oscillation, corresponding basically to a single pulse, is visible at $250 \text{ s} < t < 600 \text{ s}$. This pulse results from fast magnetosonic waves which reached the detection region while initially propagating outside the loop in the ambient medium. This corresponds to the same excitation mechanism as acted in Fig. 2.

The density enhancement marked by the red-yellow spot in Fig. 3 between $t = 700 \text{ s}$ and $t = 900 \text{ s}$ corresponds to the slow wave that propagates within the loop from the left foot-point towards the loop summit. This time lag is associated with the period $l/2c_s \approx 950 \text{ s}$, where l is the loop length, which would be obtained if the pulse was launched exactly at the foot-point. Whereas for a pulse launched at $x_0 = 0, z_0 = 0$ the main force exerted on the loop is perpendicular to the field lines, a pulse launched close to one footpoint also accelerates gas along the field lines, giving rise to a slow-mode pulse traveling along the loop from the footpoint nearest to the initial location of the pulse. As shown by Selwa et al. (2005a) an initial pulse launched asymmetrically and closer to one footpoint efficiently generates the fundamental mode of slow standing waves, while a pulse launched symmetrically or almost symmetrically generates mainly the first harmonic slow standing wave.

It is noteworthy that mass is redistributed due to the slow wave from the location where the pulse hits the loop to the other end of the loop, i.e. from one foot-point to the other for asymmetric excitations, and from the apex to the foot-points for symmetric excitations. Such redistributions for symmetric and asymmetric pulses are shown in Fig. 4. As was shown the speed of such a redistribution is the slow mode speed. It is noteworthy that a pulse is more clearly identified for the larger values of $|x_0|$, where the slow mode propagates along the loop from one footpoint to another, rarifying one part of the loop and compressing another. For symmetric excitations ($x_0 = 0$) the slow mode looks basically like mass sliding from the apex to footpoints. Another interesting feature is the density antinode (depression) position along $x_0 = 0$ only for the case of a symmetric excitation (which is clearly visible as a lower density region in the top panel of Fig. 4). In the case of asymmetric excitation such antinodes are located in the foot-points and we observe them as a rarified region at one foot-point and an enhanced region at another.

Wave period P and ratio P/τ vs normalized pulse position $|x_0/L_f|$ are shown in Fig. 5. It is noteworthy that P grows and τ/P decreases with $|x_0|$. Consequently, an initial pulse that is launched on the line $z_0 = 0$ farther out from the symmetrical position $x_0 = 0$ excites longer period waves which are more strongly attenuated.

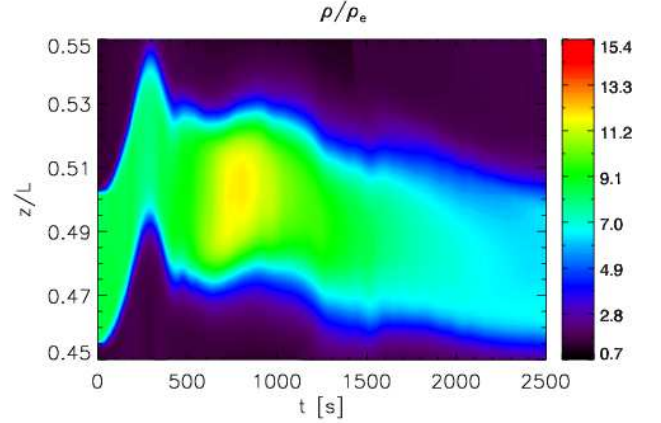


Figure 3. Time-signature of the mass density triggered by the initial pulse launched at $x_0 = -42 \text{ Mm}$, $z_0 = 0$. Compare with Fig. 2 for which $x_0 = 0$.

3.3. Energy leakage as attenuation mechanism

We expect that larger period waves are more weakly attenuated by a classical attenuation phenomenon like viscosity. As the applied MHD equations are ideal and numerical diffusion is small, viscosity is not present here. We infer that the mechanism of wave attenuation acting in these simulations differs from viscous attenuation. Here we explore and test the conjecture that attenuation is due to energy leakage. Longer wavelength waves experience more difficulties in fitting into a curved loop structure and as a result they leak energy into the ambient medium (Wentzel 1974). This process leads to a decrease of the wave amplitude - a process which is characteristic of wave attenuation. These findings are in general agreement with the results of Murawski & Roberts (1993), who studied energy leakage of normal modes in coronal structures.

Evidence of energy leakage from the loop is provided by perturbed energy density profiles (Fig. 6). The position of the loop corresponds to the white contour at the bottom of the figures. The first maximum from the top, represented by a pink-white patch, results from the initial pulse, but other maxima are a consequence of the energy leakage (red areas outside the loop). Additional evidence that energy leaks from the loop via fast magnetosonic waves is provided by the perturbations in the thermal and magnetic pressures are in-phase out of the loop.

4. SUMMARY AND DISCUSSION

The results we obtained in this paper can be summarized as follows. Broadly speaking three main classes of results arise from the simulations: those concerning the excitation of different wave modes in a curved loop by an external pulse, those related to the attenuation and those con-

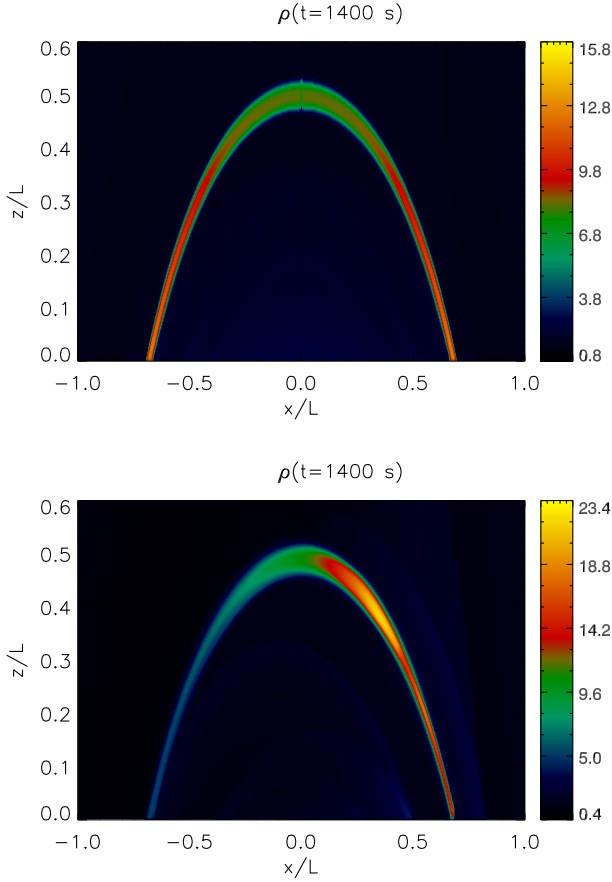


Figure 4. Distribution of the mass along the loop for a pulse launched at $x_0 = z_0 = 0$ (top panel) and $x_0 = -0.42 L$, $z_0 = 0$ (bottom panel).

cerning the asymptotic net displacement of the plasma column. From what we presented, the former two appear more prominent, convincing and, in our opinion, original. The last-named results are due to nonlinearity: the column is not only displaced, but it is dissolved in time. The column is displaced as the whole loop structure attains a different equilibrium. Foot-points move apart and as a consequence the structure expands. We have presented evidence that within the confines of a 2-D model the different observed loop modes (kink, longitudinal, sausage) are all excited by the same external pulse, but their relative strengths/amplitudes depend on the pulse location. We have verified that numerical diffusion is small and have conjectured that wave leakage is the physical process which is responsible for this feature.

There are also further conclusions: τ/P remains smaller than observed, irrespective of the chosen parameters. This suggests that there are still some significant differences between observed and modeled loops (e.g. gravity). The fact that τ/P decreases rapidly as the location of the pulse moves from $x_0 = 0$ to larger $|x_0|$, associated with a decrease in kink amplitude, suggests that a

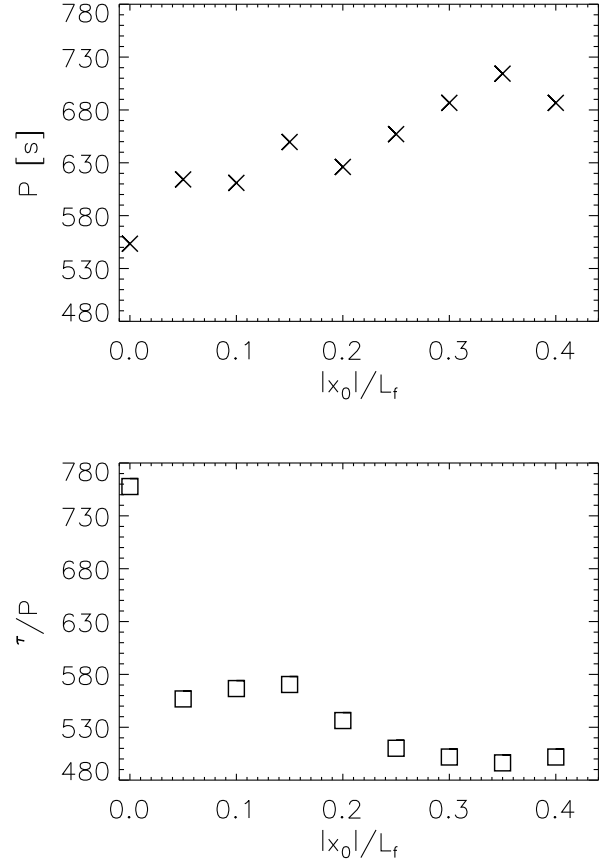


Figure 5. Period P (top panel) and the ratio of attenuation time τ to period, τ/P (bottom panel), vs normalized pulse position $|x_0|/L_f$.

pulse near $x_0 = 0$ is needed to produce vertical loop oscillations that can be clearly observed. Note that for $\tau/P < 0.2$ the oscillation appears basically like a single kink and will not be identified as an oscillation in the observational data. Since the pulse must be launched below the loop itself (in 3-D geometry) for a vertical oscillation, the choice of location of the pulse is quite limited. This may well be one reason why vertical oscillations of loops were not discovered earlier: they may be rare.

We also conclude that energy leakage from the loop into the ambient medium may be the main mechanism responsible for attenuation of vertical kink oscillations.

ACKNOWLEDGMENTS

MS expresses her thanks to the conference organizers for their financial support. KM expresses his sincere thanks to Dr. Luigi Nocera for stimulating discussions. MS thanks Dr. Robert Cameron for his helpful comments. The magnetohydrodynamic code used in this study was

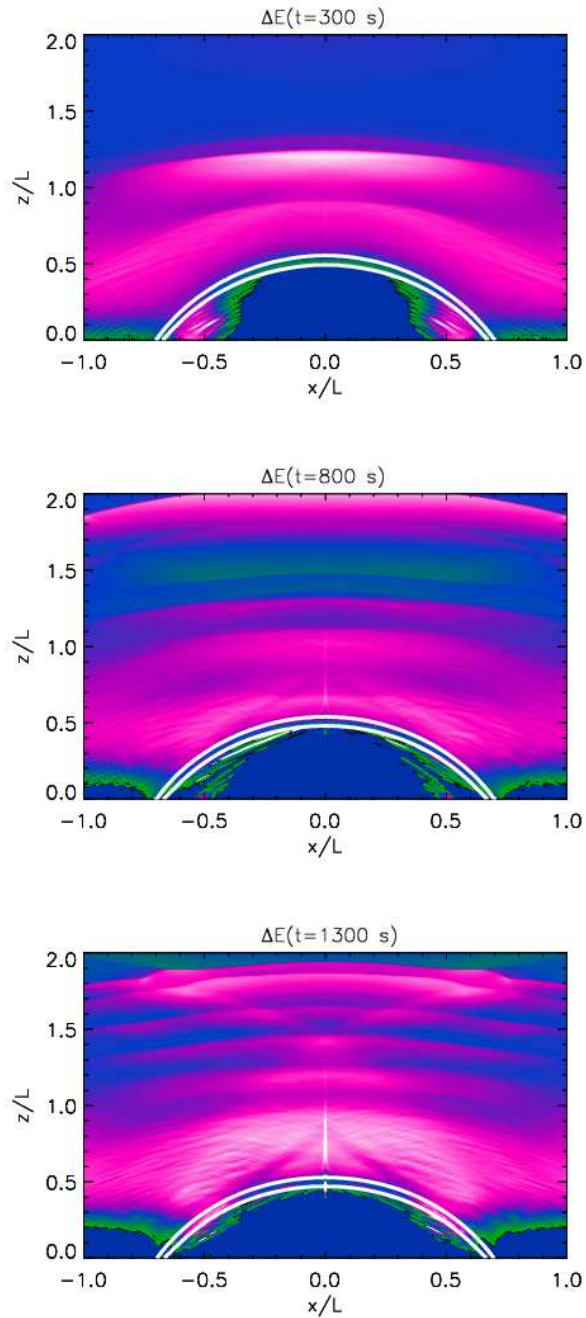


Figure 6. Evolution of perturbed energy beyond the loop showing energy leakage ($t = 300$ s - top panel, $t = 800$ s - middle panel, $t = 1300$ s - bottom panel) in the case of $A_p = 15 p_e$ and $x_0 = z_0 = 0$.

developed at the University of Washington by Ogden S. Jones, Uri Shumlak, Scott Eberhardt, Bogdan Udrea, and provided through the sponsorship of AFOSR program. MS's & KM's work was financially supported by a grant from the State Committee for Scientific Research Republic of Poland, with KBN grant No. 2 PO3D 016 25.

REFERENCES

- [1] Aschwanden M., Fletcher L., Schrijver C., Alexander D. 1999, ApJ, 520, 880
- [2] del Zanna L., Schaekens E., Velli M. 2005, A&A, 431, 1095
- [3] Jones O.S., Shumlak U., Eberhardt D. S. 1997, J. Comput. Phys., 130, 231
- [4] Murawski K., Roberts B. 1993, Solar Phys., 143, 89
- [5] Murawski K., Selwa M., Rossmanith J.A. 2005a, Solar Phys., in press
- [6] Murawski K., Selwa M., Nocera L. 2005b, A&A, 437, 687
- [7] Selwa M., Murawski K., Solanki S.K. 2005a, A&A, 436, 701
- [8] Selwa M., Murawski K., Solanki S.K., Wang T.J., Tóth G. 2005b, A&A, 440, 385
- [9] Smith J.M., Roberts B., Oliver R. 1997, A&A, 317, 752
- [10] Wang T.J., Solanki S.K. 2004, A&A, 421, L33
- [11] Wang T.J., Solanki S.K., Curdt W., Innes D.E., Dammash I.E., ApJ, 574, L101 (2002)
- [12] Wentzel D.G., Solar Phys., 39, 129 (1974)